Generalized Multiple-Mode OFDM With Index Modulation

Miaowen Wen, *Senior Member, IEEE*, Qiang Li, Ertugrul Basar, *Senior Member, IEEE*, and Wensong Zhang

***Abstract*— Multiple-mode orthogonal frequency division multiplexing with index modulation (MM-OFDM-IM), which transmits an OFDM signal with information bits embedded onto multiple distinguishable signal constellations of the same cardinality and their permutations, is a recently proposed IM technique in the frequency domain. It is capable of achieving higher spectral efficiency and better error performance than classical OFDM and existing frequency-domain IM schemes. In this paper, we propose the scheme of generalized (G-) MM-OFDM-IM, which allows a different subcarrier to utilize a signal constellation of a different size while conveying the same number of IM bits. Considering phase shift keying constellations, we present design guidelines for GMM-OFDM-IM to achieve an optimal error performance in the asymptotically high signal-to-noise ratio region. A computationally efficient and near-optimal detector based on the idea of sequential decoding is also tailored to GMM-OFDM-IM, which avoids the detection of an illegitimate constellation permutation. Monte Carlo simulations are conducted to validate the inherent properties and advantages of GMM-OFDM-IM.**

***Index Terms*— Index modulation, OFDM, multiple constellations, sequential decoding, bit error rate.**

I. Introduction

INDEX modulation (IM) is a novel digital modulation concept that relies on the indices of some building blocks of communication systems to convey information [1]–[3]. For its appealing advantages such as high energy efficiency and superior bit error rate (BER) performance, IM has been widely recognized as a candidate modulation technique for next-generation wireless networks [4]–[6]. Recently, a great deal of effort has been poured into developing a special realization of IM by exploring the orthogonal frequency division multiplexing (OFDM) subcarriers. The first attempt was made in [7], where the proposed scheme is termed as subcarrier-index modulation (SIM-) OFDM. In SIM-OFDM, the incoming bits are split into two bit streams; then, each bit of the first bit stream is assigned to a subcarrier and the subcarriers associated with the majority bit value are modulated by the second bit stream. A BER performance improvement was reported in [7], but it was also revealed therein that SIM-OFDM would suffer from the error propagation once a subcarrier status is erroneously detected. To solve this problem, an enhanced (E-)SIM-OFDM scheme was proposed in [8], whose idea is to confine the possible detection error within a pair of subcarriers by using an information bit to indicate one active subcarrier between them. In fact, ESIM-OFDM is a special representation of what was termed later in [9] as OFDM-IM.

In OFDM-IM, the total OFDM subcarriers are divided equally into several subcarrier groups to perform IM independently, where the size of each group is denoted by n and is not limited to two as in ESIM-OFDM. For each subcarrier group, the information bits are loaded onto both the conventional M-ary modulation symbols carried on a active subcarriers and the subcarrier activation patterns (SAPs) of number $2^{\lfloor \log_2 \ C(n,a) \rfloor}$, where $C(\cdot,\cdot)$ and $\lfloor \cdot \rfloor$ stand for the binomial coefficient and the floor function, respectively. The information bits can be recovered by either the maximum-likelihood (ML) detector or log-likelihood ratio (LLR) detector in [9], where the latter can exhibit similar performance to the former with a significantly reduced computational complexity as low as that of the classical OFDM single-tap receiver. The advantages of OFDM-IM over conventional OFDM in terms of BER and flexibility in system configuration were verified in [9], and these triggered several follow-up studies in recent times.

Instead of the lexicographic ordering in [9], the authors of [10] suggested sorting the SAPs in such a manner that all subcarriers are activated equiprobably, which dispenses with the channel state information (CSI) at the transmitter. At the cost of a feedback link, a better system performance was obtained by selecting those SAPs favorable for IM according to the CSI in [11]. The above three bits-to-SAP mapping methods explore different subspaces of the full space expanded by $C(n,a)$ SAPs, and would probably decide on any of the $C(n,a) - 2^{\lfloor \log_2 \ C(n,a) \rfloor}$ illegal SAPs from the complementary space when coupled with the LLR receiver or the proposed greedy receiver in [12] that determines the status of the subcarriers by measuring their received power. To avoid the

Manuscript received January 25, 2018; revised May 27, 2018 and July 3, 2018; accepted July 16, 2018. Date of publication August 6, 2018; date of current version October 9, 2018. This work was supported in part by the National Natural Science Foundation of China under Grant 61501190, in part by the Natural Science Foundation of Guangdong Province under Grant 2018B030306005, in part by the Turkish Academy of Sciences Outstanding Young Scientist Award (TUBA-GEBIP) Programme, in part by the Pearl River Nova Program of Guangzhou under Grant 201806010171, and in part by the Open Research Fund of National Mobile Communications Research Laboratory, Southeast University, under Grant 2017D08. The associate editor coordinating the review of this paper and approving it for publication was R. He. *(Corresponding author: Miaowen Wen.)*

M. Wen is with the School of Electronic and Information Engineering, South China University of Technology, Guangzhou 510640, China, and also with the National Mobile Communications Research Laboratory, Southeast University, Nanjing 210096, China (e-mail: eemwwen@scut.edu.cn).

Q. Li and W. Zhang are with the School of Electronic and Information Engineering, South China University of Technology, Guangzhou 510640, China (e-mail: eeqiangli@mail.scut.edu.cn; eez.wensong@mail.scut.edu.cn).

E. Basar is with the Communications Research and Innovation Laboratory, Department of Electrical and Electronics Engineering, Koç University, Istanbul 34450, Turkey (e-mail: ebasar@ku.edu.tr).

Color versions of one or more of the figures in this paper are available online at http://ieeexplore.ieee.org.

Digital Object Identifier 10.1109/TWC.2018.2860954

illegal SAP detection, a novel scheme was proposed in [13] by encoding all $C(n, a)$ SAPs with a variable length of bits, which, however, requires the transceiver to adapt the modulation type to the unbalanced bits-to-SAP mapping. Different subcarrier grouping methods may lead to different system performance for OFDM-IM as the detection accuracy of the IM bits as well as the conventional modulation (CM) bits highly depends on the channel quality, and the studies from the perspective of both BER optimality [14] and achievable rate optimality [15], [16] proved that the subcarrier-level interleaving is the best choice. The achievable rate performance was analyzed in [16], where it is found that OFDM-IM is capable of outperforming conventional OFDM under finite-alphabet input by judiciously choosing the number of active subcarriers a and the modulation order M. This important observation was later reconfirmed in [17], and the guideline for the selection of OFDM-IM system parameters was also designed therein. An upper bound on the BER of OFDM-IM under perfect and imperfect CSI conditions was first derived according to the union bounding technique in [9], which reveals that the IM bits generally have better protection than the CM bits. Later in [18], a tighter BER upper bound was presented, which is able to isolate the effects of IM and CM on the system's error performance. Unlike [9] and [18] that considered ML detection, the studies of [19] and [20] undertook the BER analysis with respect to various CSI conditions by assuming a greedy receiver and discovered that the greedy receiver can achieve nearly optimal error performance for a large value of M, or even outperform the ML receiver under CSI uncertainty. It is understandable that as classical OFDM, OFDM-IM is also vulnerable to carrier frequency offset (CFO) and/or Doppler shifts due to the nature of orthogonal multi-carrier transmission. Fortunately, the resulting intercarrier interference (ICI) imposes less detrimental effect on OFDM-IM than the classical OFDM thanks to the presence of empty subcarriers in OFDM-IM [21]. Recently, the authors of [22] implemented OFDM-IM for the first time by using the software defined radio technology and corroborated its suitability to real-time applications.

Besides the exploration of the inherent properties and practical implementation as mentioned above, there also have been many studies that focus on the performance improvement of OFDM-IM systems. Aiming at suppressing ICI, the integration of OFDM-IM with the ICI self-cancellation technique and transceiver linear processing were proposed in [23] and [24], respectively. In [25], the coordinate interleaving technique was applied to a pair of active subcarriers, enhancing the protection of the CM bits and further harvesting an additional diversity gain for the OFDM-IM system. Another effective method for obtaining diversity gain through linear precoding of two modulated symbols was proposed for OFDM-IM in [26]. To counteract the unreliable detection of the subcarrier status at low signal-to-noise ratio (SNR), the authors of [27] and [28] proposed two novel schemes for OFDM-IM by transmitting a repeated SAP across multiple subcarrier groups and encoding the IM bits according to a predesigned trellis, respectively. To compensate the deficiency that the number of the IM bits increases combinatorially rather than linearly as that of the CM bits, several countermeasures have been taken to improve the spectral efficiency (SE) of the OFDM-IM system [29]–[33]. Concretely, two generalizations of OFDM-IM were designed in [29]: one allows a flexible number of active subcarriers, transmitting more IM bits, and the other one extends IM to both the in-phase (I-) and quadrature (Q-) components of the OFDM signal, doubling the number of IM bits. The latter, termed as OFDM-I/Q-IM in [30], was proved to achieve a more than double SNR gain over conventional OFDM compared with OFDM-IM for an SE of 2 bps/Hz. In [31] and [32], OFDM-IM was combined with the multi-input-multi-output (MIMO) technique to increase the number of IM bits proportionally to that of the transmit antennas, and several efficient detectors were tailored to enable low-complexity implementation. By introducing a virtual vector of size much larger than that of a subcarrier group, a compressed sensing-assisted signaling strategy, which is able to enlarge the index domain of OFDM-IM, was proposed in [33].

More recently, great attention has been paid to the use of multiple signal constellations for IM owing to its advantage in significantly improving the SE and/or transmit diversity of OFDM-IM systems. The first example with two signal constellations (primary and secondary ones) was presented in [34], where the entire signal processing procedure follows the one of OFDM-IM except that the "inactive" subcarriers transmit signals from a non-zero signal constellation (secondary one) that is distinguishable from the primary one utilized by the "active" subcarriers, rather than the null subcarriers as in OFDM-IM. The signal constellation was also referred to as a mode in [34], and thereby the proposed scheme therein was named as dual-mode (DM-) OFDM. In [35], DM-OFDM was generalized by relaxing the constraint on the number of subcarriers using the primary signal constellation (or similarly the secondary one) at the cost of a slight performance loss. Unlike [34] and [35] that considered M-ary quadrature amplitude modulation (QAM) constellations, the study of [36] focused on M-ary phase shift keying (PSK) constellations with different power levels, which are determined based on the BER minimization via numerical simulations. Another realization of IM-aided OFDM with two non-zero signal constellations was proposed in [37], in which the same information are transmitted through both constellations instead of different information as in DM-OFDM for enhancing the diversity performance. By considering the zero-amplitude point as the third mode, the authors of [38] extended their proposed DM-OFDM to triple-mode (TR-) OFDM. To enable ease of implementation, a reduced-complexity two-stage LLR detector, which first distinguishes the active subcarriers from the empty ones and then determines the employed non-zero constellation by an active subcarrier, was also designed for TR-OFDM. In [39], a novel multiple-mode (MM-) OFDM-IM scheme that modulates n subcarriers by n distinguishable signal constellations of the same size as well as their permutations, was proposed. Therein, design guidelines for MM-OFDM-IM systems under the constraints of PSK and QAM constellations, and a low-complexity subcarrier-wise detector were also presented. Due to the capability of transmitting more IM bits with a permutational increase, MM-OFDM-IM is shown to achieve much

higher SE and better BER performance than both OFDM-IM and DM-OFDM [39]. It should be noted that MM-OFDM-IM is not a straightforward generalization of DM-OFDM since DM-OFDM transmits a mode over multiple subcarriers while MM-OFDM-IM over a single one. The direct extension of DM-OFDM to multiple modes was in fact proposed in [40], where n subcarriers are divided into L subgroups ($L = 2$ for DM-OFDM) each transmitting a different mode. However, the number of IM bits for this extension scales combinatorially as in OFDM-IM and DM-OFDM, whose increase ratio is lower than that of MM-OFDM-IM.

Adaptive modulation has also been applied to OFDM systems in order to improve their BER performance [41]–[43]. In adaptive OFDM systems, based on the channel state information (CSI) at the transmitter, the modulation order used on each subcarrier is adaptively selected considering to the fading severity of that subcarrier. Motivated by the adaptive modulation and aiming to provide a simple way for adjusting the SE, in this paper, we propose a generalization of MM-OFDM-IM, termed as generalized (G-) MM-OFDM-IM, by considering PSK constellations and relaxing the constraint on the cardinalities of the signal constellations employed by different subcarriers. As MM-OFDM-IM, GMM-OFDM-IM also enables a permutational increase of the IM bits. Different from the case of adaptive OFDM systems, in GMM-OFDM-IM, multiple signal constellations of different sizes are utilized to enhance the SE of classical OFDM systems and CSI is no longer required at the transmitter. Our major contributions are summarized as follows.

- We present a guideline to obtain n distinguishable signal constellations from a unit circle that lead to the optimal asymptotic BER performance of GMM-OFDM-IM systems constrained on the instantaneous power of each subcarrier. This design facilitates both the implementation of the transmitter and the signal detection at the receiver.
- We derive the power allocation coefficients and phase-rotated angles associated with n PSK constellations to attain the largest differentiability among the resulting n modes, with which the GMM-OFDM-IM system achieves the theoretically optimal asymptotic BER performance constrained on the average power of each subcarrier.
- We design a novel detector for GMM-OFDM-IM motivated by the sequential decoding idea that was first applied to the convolutional codes. This detector operates in the subcarrier level as the one originally proposed for MM-OFDM-IM, but unlike the latter, it avoids the decision on an illegal constellation permutation, thus achieving a performance closer to that of the ML detector with slightly increased computational complexity.

The remainder of this paper is organized in the following. Section II describes the system model of GMM-OFDM-IM. A design guideline for GMM-OFDM-IM under the same instantaneous subcarrier power constraint is given in Section III. Section IV proposes the optimal power allocation and phase rotation strategies for GMM-OFDM-IM under the average subcarrier power constraint. A low-complexity near-ML detector is designed in Section V. Section VI presents the Monte Carlo simulation results, and finally the paper is concluded in Section VII.

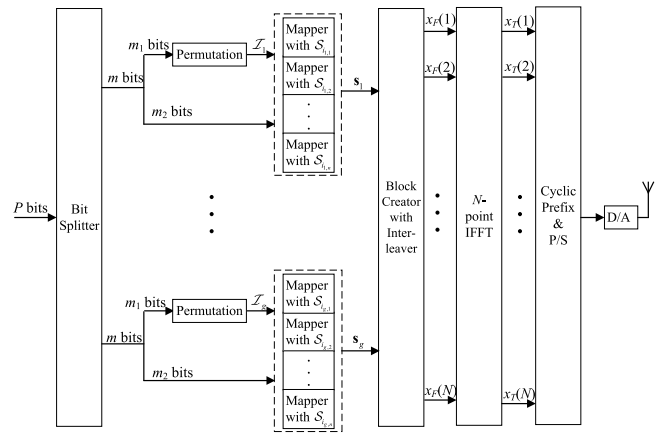

Fig. 1. Block diagram of GMM-OFDM-IM transmitter.

Notation: Scalar variables are in italic letters. Column vectors and matrices are denoted by lowercase and uppercase boldface letters, respectively. Superscript ^{T} stands for the transpose operation. $\|\cdot\|_F$ and $j = \sqrt{-1}$ refer to the Frobenius norm and the imaginary unit. $\mathbf{I}_n$ denotes the $n \times n$ identity matrix. $\mathcal{CN}(\mu, \sigma^2)$ denotes the complex Gaussian distribution with mean μ and variance σ^2. $\mathrm{diag}(\cdot)$ transforms a vector into a diagonal matrix. $\mathrm{rank}(\cdot)$ returns the rank of a matrix.

II. System Model

The GMM-OFDM-IM transmitter, which is built on the conventional OFDM architecture of N subcarriers, is depicted in Fig. 1. At the beginning, a total of P incoming bits to be transmitted via an OFDM symbol are equally split into g blocks, each containing $m = P/g$ bits, and correspondingly, the total OFDM subcarriers are divided into g groups, each comprising $n = N/g$ subcarriers. Then, one bit block modulates one subcarrier group of a size much smaller than N independently, reducing the implementation complexity of IM. For brevity, let us focus on the processing procedure associated with the γ-th bit block and subcarrier group, where $\gamma \in \{1, \ldots, g\}$. Specifically, the available m bits are further partitioned into two parts for different purposes. The first part, consisting of m_1 bits, determines the order of the sequence $\mathcal{Q}(= \{1, \ldots, n\})$, generating $\mathcal{I}_\gamma = \{i_{\gamma,1}, \ldots, i_{\gamma,\beta}, \ldots, i_{\gamma,n}\}$, where $i_{\gamma,\beta} \in \mathcal{Q}$ with $\beta \in \mathcal{Q}$. Using $\mathcal{I}_\gamma$, the mode employed by the β-th subcarrier, denoted by $\mathcal{S}_{i_{\gamma,\beta}}$, is determined as the $i_{\gamma,\beta}$-th element of a mode set $\{\mathcal{S}_1, \ldots, \mathcal{S}_n\}$. It is noteworthy that to enable IM, we have to ensure that $\mathcal{S}_\beta \cap \mathcal{S}_{\beta'} = \emptyset, \forall \beta, \beta' \in \mathcal{Q}, \beta \neq \beta'$, though they may have different constellation sizes. Without loss of generality, we assume that n_k out of n modes are M_k-ary constellations, where $\sum_{k=1}^{K} n_k = n$ and $M_1 > M_2 > \cdots > M_K$. In this paper, all modes are limited to be PSK constellations,[1] and the combination of the total n modes is

[1]Due to the inherited nature of QAM constellations, it is impossible for GMM-OFDM-IM with QAM constellations to achieve the same instantaneous subcarrier power. Moreover, for the average subcarrier power constraint, since it involves many parameters to be optimized, it is very difficult to derive the optimal mode selection under the QAM constraint. However, similar to [39], a practical mode selection for GMM-OFDM-IM under the QAM constraint can be easily obtained.

TABLE I
A LOOK-UP TABLE EXAMPLE FOR $n = 3$

m_1 bits	Permutations ($\mathcal{I}_\gamma$)	Constellations ($\mathbf{s}_\gamma$)
[0 0]	$\{1,2,3\}$	$\{\mathcal{S}_1,\mathcal{S}_2,\mathcal{S}_3\}$
[0 1]	$\{1,3,2\}$	$\{\mathcal{S}_1,\mathcal{S}_3,\mathcal{S}_2\}$
[1 0]	$\{2,1,3\}$	$\{\mathcal{S}_2,\mathcal{S}_1,\mathcal{S}_3\}$
[1 1]	$\{3,2,1\}$	$\{\mathcal{S}_2,\mathcal{S}_3,\mathcal{S}_1\}$
Illegal	$\{2,3,1\}$	$\{\mathcal{S}_3,\mathcal{S}_1,\mathcal{S}_2\}$
	$\{3,1,2\}$	$\{\mathcal{S}_3,\mathcal{S}_2,\mathcal{S}_1\}$

presented as an $\mathcal{M}$-ary constellation that is normalized to have unit average power, where $\mathcal{M} = \sum_{k=1}^{K} n_k M_k$. As an example of $(M_1(n_1), M_2(n_2), M_3(n_3)) = (8(1), 4(2), 2(1))$, we have $\{\mathcal{S}_1, \mathcal{S}_2, \mathcal{S}_3, \mathcal{S}_4\} = \{\text{8-PSK}, \text{QPSK-I}, \text{QPSK-II}, \text{BPSK}\}$, where QPSK-I and QPSK-II are two different QPSK constellations. The second part, made up of $m_2 = \sum_{k=1}^{K} n_k \log_2 M_k$ bits, is mapped to an $n \times 1$ symbol vector $\mathbf{s}_\gamma = [s_{\gamma,1}, \ldots, s_{\gamma,\beta}, \ldots, s_{\gamma,n}]^T$, where $s_{\gamma,\beta} \in \mathcal{S}_{i_{\gamma,\beta}}$. Since $\{\mathcal{S}_{i_{\gamma,1}}, \ldots, \mathcal{S}_{i_{\gamma,n}}\}$ is a full permutation of $\{\mathcal{S}_1, \ldots, \mathcal{S}_n\}$ that has $n!$ possible realizations, we have $m_1 = \lfloor \log_2 n! \rfloor$ and there are $n! - 2^{\lfloor \log_2\ n! \rfloor}$ unused (illegal) permutations. The mapping between m_1 bits and $\mathcal{I}_\gamma$ can be easily implemented through a look-up table or the permutation method.

1) *Look-Up Table Method:* In this method, a table that gives the complete mapping relationship, is stored at both the transmitter and receiver sides for inquiry. Table I presents an example for $n = 3$, where two illegal permutations are discarded.
2) *Permutation Method:* In this method, the incoming m_1 bits are first converted into a decimal integer $A \in [0, n! - 1]$ and then according to

$$A = (c_n - 1) \cdot (n-1)! + \cdots + (c_2 - 1) \cdot 1! + (c_1 - 1) \cdot 0!, \quad (1)$$

the sequence $\mathcal{A} = \{c_n, \ldots, c_1\}$ is obtained. Finally, the permutation $\mathcal{I}_\gamma$ is determined by letting $i_{\gamma,1}$ be the c_n-th element of $\mathcal{Q}$, $i_{\gamma,2}$ be the c_{n-1}-th element of the new set formed by excluding the c_n-th element from $\mathcal{Q}$, and so on. An example for $n = 3$ is given as follows.

$$\begin{aligned}
0 &= (1-1)\cdot 2! + (1-1)\cdot 1! + (1-1)\cdot 0! \rightarrow \\
&\quad \mathcal{A} = \{1,1,1\} \rightarrow \mathcal{I}_\gamma = \{1,2,3\} \\
1 &= (1-1)\cdot 2! + (2-1)\cdot 1! + (1-1)\cdot 0! \rightarrow \\
&\quad \mathcal{A} = \{1,2,1\} \rightarrow \mathcal{I}_\gamma = \{1,3,2\} \\
2 &= (2-1)\cdot 2! + (1-1)\cdot 1! + (1-1)\cdot 0! \rightarrow \\
&\quad \mathcal{A} = \{2,1,1\} \rightarrow \mathcal{I}_\gamma = \{2,1,3\} \\
3 &= (2-1)\cdot 2! + (2-1)\cdot 1! + (1-1)\cdot 0! \rightarrow \\
&\quad \mathcal{A} = \{2,2,1\} \rightarrow \mathcal{I}_\gamma = \{2,3,1\} \\
4 &= (3-1)\cdot 2! + (1-1)\cdot 1! + (1-1)\cdot 0! \rightarrow \\
&\quad \mathcal{A} = \{3,1,1\} \rightarrow \mathcal{I}_\gamma = \{3,1,2\} \\
5 &= (3-1)\cdot 2! + (2-1)\cdot 1! + (1-1)\cdot 0! \rightarrow \\
&\quad \mathcal{A} = \{3,2,1\} \rightarrow \mathcal{I}_\gamma = \{3,2,1\}. \quad (2)
\end{aligned}$$

At the receiver, the estimated permutation $\mathcal{I}_\gamma$ is first linked to A by reversing the above process. If $A \geq 2^{m_1}$, the detected $\mathcal{I}_\gamma$ is illegal and abandoned; otherwise, the m_1 bits are obtained by transforming A into the binary sequence.

After $\mathbf{s}_\gamma$ for all γ are obtained, they enter the block creator coupled with the subcarrier-level interleaver, outputting the $N \times 1$ main OFDM block

$$\begin{aligned}
\mathbf{x}_F &= [x_F(1), \ldots, x_F(N)]^T \\
&= [s_{1,1}, s_{2,1}, \ldots, s_{g,1}, s_{1,2}, s_{2,2}, \ldots, s_{g,2}, \ldots, \\
&\qquad s_{1,n}, s_{2,n}, \ldots, s_{g,n}]^T. \quad (3)
\end{aligned}$$

Then, N-point inverse fast Fourier transform (FFT) is performed on $\mathbf{x}_F$ to generate the time-domain signal $\mathbf{x}_T = [x_T(1), \ldots, x_T(N)]^T$. A length-$G$ cyclic prefix (CP) $[x_T(N-G+1), \ldots, x_T(N)]^T$ is further appended at the beginning of $\mathbf{x}_T$, and the resulting signal is fed into parallel-to-serial (P/S) and digital-to-analog (D/A) converters successively. Finally, the output signal is emitted into the frequency-selective Rayleigh fading channel, whose time-domain channel impulse response is given by

$$\mathbf{h}_T = [h_T(1), \ldots, h_T(\nu)]^T, \quad (4)$$

where $\nu \leq G$ and each entry of $\mathbf{h}_T$ follows the distribution $\mathcal{CN}(0, 1/\nu)$. We denote the frequency-domain channel transfer function (CTF) by $\mathbf{h}_F = [h_F(1), \ldots, h_F(N)]^T$, which is the N-point FFT of $\bar{\mathbf{h}}_T$, where $\bar{\mathbf{h}}_T$ is a length-N vector given by $\bar{\mathbf{h}}_T = [\mathbf{h}_T{}^T, 0, \ldots, 0]^T$.

At the receiver side, the CP is first removed from the received signal. Subsequently, N-point FFT and de-interleaving operations are carried out in sequence, yielding the frequency-domain received signal associated with the γ-th subcarrier group

$$\mathbf{y}_\gamma = [y_\gamma(1), \ldots, y_\gamma(n)]^T = \mathbf{X}_\gamma \mathbf{h}_\gamma + \mathbf{w}_\gamma, \quad (5)$$

where $\mathbf{X}_\gamma = \text{diag}(\mathbf{s}_\gamma)$, $\mathbf{h}_\gamma = [h_F(\gamma), h_F(\gamma+g), \ldots, h_F(\gamma+(n-1)g)]^T$ refers to the frequency response vector associated with the γ-th subcarrier group, and $\mathbf{w}_\gamma$ is the noise vector in the frequency domain with the distribution $\mathcal{CN}(\mathbf{0}, N_0\mathbf{I}_n)$. The average received SNR per subcarrier is defined as $\rho = 1/N_0$. Note that after de-interleaving, the correlation among the elements of $\mathbf{h}_\gamma$ is significantly attenuated, and as a result it is reasonable to assume $\mathbf{h}_\gamma \sim \mathcal{CN}(\mathbf{0}, \mathbf{I}_n)$.

A straightforward solution to recover the transmitted bits is the ML detection, which can be formulated based on (5) as

$$(\hat{\mathcal{I}}_\gamma, \hat{\mathbf{s}}_\gamma) = \underset{\mathcal{I}_\gamma, \mathbf{s}_\gamma}{\arg\min} \|\mathbf{y}_\gamma - \mathbf{X}_\gamma \mathbf{h}_\gamma\|_F^2, \quad (6)$$

where $\hat{\mathcal{I}}_\gamma$ and $\hat{\mathbf{s}}_\gamma$ are the estimates of $\mathcal{I}_\gamma$ and $\mathbf{s}_\gamma$, respectively. Since there are approximately $n!$ possible realizations of $\mathcal{I}_\gamma$ and $\prod_{k=1}^{K} M_k{}^{n_k}$ possible realizations of $\mathbf{s}_\gamma$, the computational complexity of (6) in terms of complex multiplications is of order $\sim \mathcal{O}(n! \prod_{k=1}^{K} M_k{}^{n_k})$ per subcarrier group. To decrease the computational burden to the receiver, we derive a low-complexity detector, which will be introduced in Section V.

From above, without taking into account the CP cost, the SE of GMM-OFDM-IM systems, measured by bps/Hz, is given by

$$\mathcal{F} = \frac{m_1 + m_2}{n} = \frac{1}{n}\left(\lfloor \log_2 n! \rfloor + \sum\nolimits_{k=1}^{K} n_k \log_2 M_k\right), \quad (7)$$

from which we observe that GMM-OFDM-IM is able to provide a more flexible choice for SE by adjusting n_k and M_k, compared with MM-OFDM-IM.

For given values of n_k and $M_k, k = 1, \ldots, K$, or equivalently given a desired SE of the system, how to choose appropriate modes $\mathcal{S}_1, \ldots, \mathcal{S}_n$ that lead to the optimal BER performance and simple symbol modulation/demodulation are key issues for GMM-OFDM-IM systems. In the following two sections, we will solve this practical problem.

III. Design Guideline With Same Instantaneous Subcarrier Power Constraint

In this section, we design guidelines for mode selection under the constraint that all subcarriers transmit with the same instantaneous power, which means all $\mathcal{M}$ signal points are located on a unit circle, i.e., $r_1 = \cdots = r_K = 1$, where r_k is the radius of the M_k-ary circle constellation. This same instantaneous subcarrier power constraint enables the receiver to detect the modes merely by examining the phase of the equalized signal, significantly facilitating the practical implementation.

According to the analysis in [39], the optimal modes should maximize the minimum Euclidean distance (MED)

$$d_1 = \min_{\mu,\upsilon\in\{1,\ldots,2^m\}} \left\|\mathbf{X}_\gamma^{(\mu)} - \mathbf{X}_\gamma^{(\upsilon)}\right\|_F^2, \quad s.t.\ |s_{\gamma,\beta}|^2 = 1, \mathrm{rank}\left(\mathbf{X}_\gamma^{(\mu)} - \mathbf{X}_\gamma^{(\upsilon)}\right) = r_{\min}, \quad (8)$$

where $\mathbf{X}_\gamma^{(\mu)}$ and $\mathbf{X}_\gamma^{(\upsilon)}$ are two different realizations of $\mathbf{X}_\gamma$, and $r_{\min} = \mathrm{rank}(\mathbf{X}_\gamma^{(\mu)} - \mathbf{X}_\gamma^{(\upsilon)})$ is the diversity order achieved by GMM-OFDM-IM systems. It follows that $r_{\min} = 1$, which means in the high SNR region, the mode permutation is likely to be detected correctly and the errors mainly result from the signal point detection within a single mode. Therefore, d_1 is termed as the minimum intra-mode distance (MIAD) and maximizing it leads to the optimal BER performance of GMM-OFDM-IM systems at high SNR. Recall that on a circle, the uniformly distributed signal points have the maximum MED. The M_k-ary constellation should be the ordinary M_k-PSK constellation, which has an MIAD of $\sqrt{2 - 2\cos(2\pi/M_k)}$. Since the rotation of a signal constellation does not change its average power and MED, the number of signal constellations satisfying (8) is typically larger than n.

The criterion of (8) only considers the high SNR cases, which, however, does not necessarily ensure satisfactory BER performance in the medium SNR region. To leverage the BER performance at medium SNR, we should select n modes from those candidates provided by (8), which maximize the MED at a diversity order of two [39]

$$d_2 = \min_{\mu,\upsilon\in\{1,\ldots,2^m\}} \left\|\mathbf{X}_\gamma^{(\mu)} - \mathbf{X}_\gamma^{(\upsilon)}\right\|_F^2, \quad s.t.\ |s_{\gamma,\beta}|^2 = 1, \mathrm{rank}\left(\mathbf{X}_\gamma^{(\mu)} - \mathbf{X}_\gamma^{(\upsilon)}\right) = 2, \quad (9)$$

where for its nature d_2 is termed as the minimum inter-mode distance (MIRD). The second-order diversity is controlled by two error events: 1) any two symbols are erroneously detected as another two symbols belonging to the same two modes; 2) the permutation of any two modes is erroneously detected. The probability of the first error event depends on the MIAD and can be also minimized based on the criterion of (8). Therefore, with the result of (8) as the input, the problem of the MIRD maximization described in (9) is equivalent to the problem of the minimization of the probability of the second error event. Under the same instantaneous subcarrier power constraint, this equivalent problem can be solved by rotating n ordinary PSK constellations with some carefully designed angles. To show this, we first put forward the following theorem.

Theorem 1: The $\mathcal{M}$ signal points constructed by the optimal n modes must be taken from the regular normalized ηM_1-ary PSK constellation, in which two adjacent signal points are separated by an angle of $2\pi/\eta M_1$, and the maximum MIRD is given by $\sqrt{2 - 2\cos(2\pi/\eta M_1)}$, where η is the minimum integer satisfying $\eta M_1 \geq \mathcal{M}$.

Proof: According to (8), the M_k-ary constellation should be the ordinary M_k-PSK constellation for $k = 1, \ldots, K$. Recall that M_1/M_k is always equal to an integer power of two, and the M_1-PSK constellation subsumes any of the M_k-PSK constellations, where $k = 2, \ldots, K$. Moreover, to satisfy (9), the $\mathcal{M}$ signal points are required to be distributed as uniformly as possible. Therefore, in order to maximize the MED of the combined $\mathcal{M}$-ary constellation, the optimal n modes must be taken from the regular ηM_1-PSK constellation, which provides the maximum MIRD value of $\sqrt{2 - 2\cos(2\pi/\eta M_1)}$. ■

Based on Theorem 1, the desired n modes can be extracted from the regular ηM_1-ary PSK constellation. For ease of implementation, it is preferred to derive n_k different M_k-PSK constellations starting from $k = 1$ to $k = K$ sequentially. The detailed procedure is summarized in Algorithm 1, where the mode of M_k signal points is represented by M_k indices of the signal points of the ηM_1-PSK constellation. Besides, Algorithm 1 is designed with the assumption that two immediately adjacent signal points of the ηM_1-PSK constellation are given consecutive indices. Hence, one would obtain a different output in Algorithm 1 if a different indexing of the ηM_1-PSK constellation points is used though the MIAD

Algorithm 1 Mode Selection for GMM-OFDM-IM With Same Instantaneous Subcarrier Power

Input: n_k and M_k, $k = 1, \ldots, K$
Initialization: Let $\Theta = \{1, 2, \ldots, \eta M_1\}$ be the index set of the total signal points of the regular ηM_1-PSK constellation;
Calculate $\xi = \{\eta, \eta M_1/M_2, \ldots, \eta M_1/M_K\}$;
for $k = 1 : K$ **do**
  $I_{\kappa,M_k}(l) = \Theta(\kappa) + \xi(k)l, \kappa = 1, \ldots, n_k, l = 0, \ldots, M_k - 1$, where $I_{\kappa,M_k}(l)$ denotes the index of the l-th signal point of the κ-th M_k-PSK constellation;
  Update $\Theta = \Theta \backslash \{I_{1,M_k}, \ldots, I_{n_k,M_k}\}$;
end for
Output: $I_{\kappa,M_k}(l)$ for $k = 1, \ldots, K, \kappa = 1, \ldots, n_k$ and $l = 0, \ldots, M_k - 1$

TABLE II

AN EXAMPLE OF MODE SELECTION FOR $(M_1(n_1), M_2(n_2), M_3(n_3)) = (8(1), 4(2), 2(1))$

Mode	Indices
$\mathcal{S}_1$	$\{1, 4, 7, 10, 13, 16, 19, 22\}$
$\mathcal{S}_2$	$\{2, 8, 14, 20\}$
$\mathcal{S}_3$	$\{3, 9, 15, 21\}$
$\mathcal{S}_4$	$\{5, 17\}$

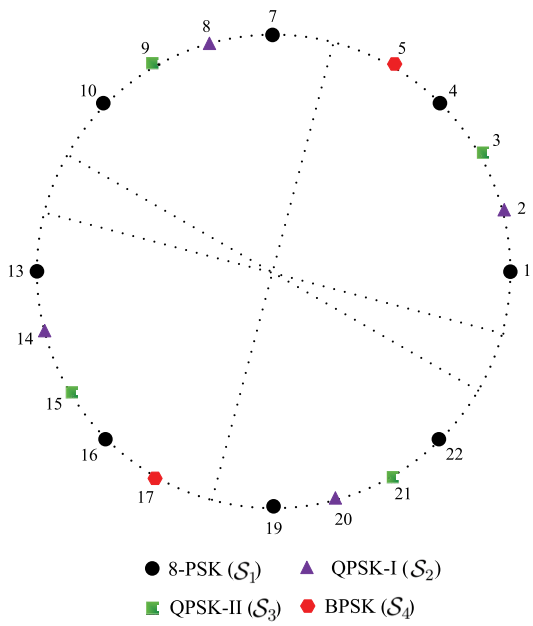

Fig. 2. Four optimal modes with $(M_1(n_1), M_2(n_2), M_3(n_3)) = (8(1), 4(2), 2(1))$ under the same instantaneous subcarrier power constraint.

and MIRD always remain the same. For all demonstrative examples in this paper, the indices are counted counter-clockwise with the first signal point located on the positive x-axis. For example, when $(M_1(n_1), M_2(n_2), M_3(n_3)) = (8(1), 4(2), 2(1))$, it follows that $\eta = 3$, and according to Algorithm 1, we can obtain the optimal four modes, which are listed in Table II and depicted in Fig. 2 as well.

IV. DESIGN GUIDELINE WITH AVERAGE SUBCARRIER POWER CONSTRAINT

As analyzed in Section III, under the same instantaneous subcarrier power constraint, all modes are packed on a unit circle. This is advantageous for practical implementation, but does not necessarily result in theoretically minimum BER. In pursuit of the optimal BER performance, in this section, we relax the constraint on the instantaneous subcarrier power and focus on the design of the mode selection guideline with $\sum_{k=1}^{K} n_k M_k r_k^2 = \mathcal{M}, r_1 \neq r_2 \neq \cdots \neq r_K$.

In order to enlarge the MED, it is heuristic to allocate more power to higher-order signal constellations and less power to lower-order ones, namely $r_1 > r_2 > \cdots > r_K$. Although n modes can vary in power, by following the criterion of (8), each of them is expected to be the ordinary PSK constellation, as discussed in Section III. Their associated radii $r_1, \ldots, r_K$ can be determined by minimizing the asymptotic BER of GMM-OFDM-IM systems.

At high SNR, the BER of GMM-OFDM-IM systems can be approximated by [39]

$$\begin{aligned} P_e &\approx \frac{1}{m} \sum_{k=1}^{K} n_k P_b\left(M_k, r_k\right) \log_2 M_k \\ &\approx \frac{1}{m} \sum_{k=1}^{K} n_k P_s\left(M_k, r_k\right), \quad s.t. \sum_{k=1}^{K} n_k M_k r_k^2 = \mathcal{M}, \end{aligned} \tag{10}$$

where $P_b(M_k, r_k)$ and $P_s(M_k, r_k)$ are the bit and symbol error probabilities of M_k-PSK demodulation over the Rayleigh fading channel, respectively. Since $P_s(M_k, r_k)$ can be tightly upper bounded by [44]

$$\begin{aligned} P_s\left(M_k, r_k\right) &\leq \frac{M_k - 1}{M_k} \frac{1}{1 + \rho r_k^2 g\left(M_k\right)} \\ &< \frac{M_k - 1}{M_k} \frac{1}{\rho r_k^2 g\left(M_k\right)}, \end{aligned} \tag{11}$$

where $g(M_k) = \sin^2(\pi/M_k)$, the optimization of $r_k, k = 1, \ldots, K$, can be formulated as

$$\begin{aligned} \{r_{opt,1}, \ldots, r_{opt,K}\} = \min_{r_1, \ldots, r_K} & \sum_{k=1}^{K} \frac{M_k - 1}{M_k} \frac{n_k}{\rho r_k^2 g\left(M_k\right)}, \\ s.t. & \sum_{k=1}^{K} n_k M_k r_k^2 = \mathcal{M}. \end{aligned} \tag{12}$$

We give the following theorem on the radii of the considered modes to achieve the optimal asymptotic BER performance.

Theorem 2: The minimum asymptotic BER of GMM-OFDM-IM systems is achieved only and if only the corresponding radii satisfy

$$r_1^2 = \frac{\mathcal{M}}{\sum_{k=1}^{K} n_k M_k Z_k}, \quad r_k^2 = r_{k-1}^2 T_k, \ k = 2, \ldots, K, \tag{13}$$

where $Z_k = \prod_{\iota=1}^{k} T_\iota$ with

$$T_k = \begin{cases} 1, & k = 1 \\ \dfrac{M_{k-1}}{M_k} \sqrt{\dfrac{g\left(M_{k-1}\right)\left(M_k - 1\right)}{g\left(M_k\right)\left(M_{k-1} - 1\right)}}, & k = 2, \ldots, K. \end{cases} \tag{14}$$

Proof: We resort to the method of Lagrange multipliers to solve the optimization problem of (12). To start with, let us define the Lagrange function

$$\begin{aligned} \mathcal{L}\left(r_1^2, \ldots, r_K^2, \lambda\right) = & \sum_{k=1}^{K} \frac{M_k - 1}{M_k} \frac{n_k}{\rho r_k^2 g\left(M_k\right)} \\ & - \lambda \left(\sum_{k=1}^{K} n_k M_k r_k^2 - \mathcal{M} \right), \end{aligned} \tag{15}$$

where λ is the Lagrange multiplier. Solving $K + 1$ equations in $K + 1$ unknowns

$$\begin{cases} \dfrac{\partial \mathcal{L}\left(r_1^2, \ldots, r_K^2, \lambda\right)}{\partial r_k^2} = 0, \quad k = 1, \ldots, K \\ \displaystyle\sum_{k=1}^{K} n_k M_k r_k^2 = \mathcal{M} \end{cases} \tag{16}$$

yields (13), completing the proof. ■

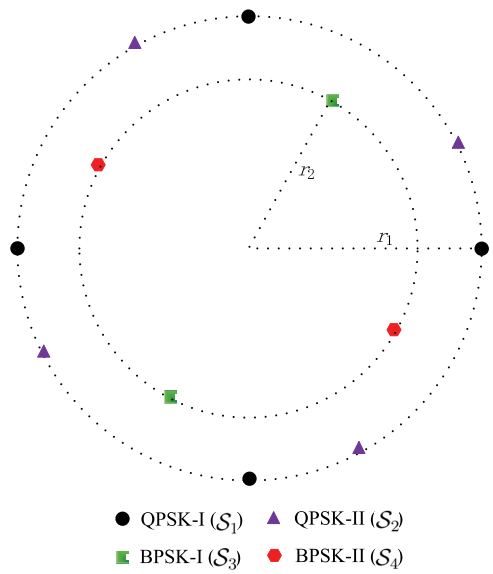

Fig. 3. Four optimal modes for $(M_1(n_1), M_2(n_2)) = (4(2), 2(2))$ under average subcarrier power constraint.

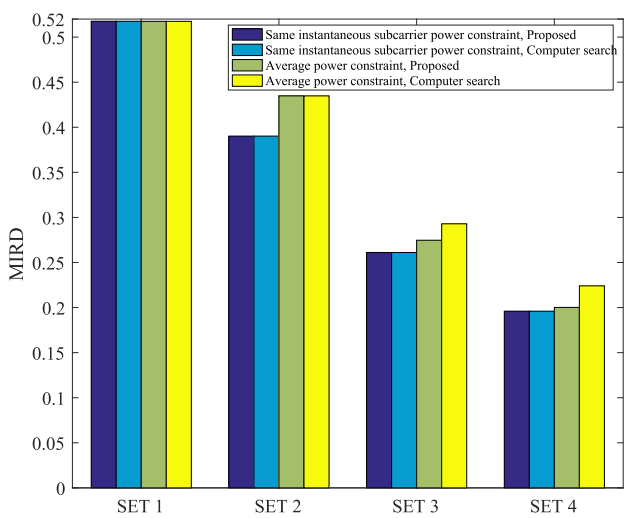

Fig. 4. Comparison of MIRDs derived from computer simulations and proposed design with the same instantaneous subcarrier and average subcarrier power constraints.

After obtaining $r_1, \ldots, r_K$, the next step is to assign a proper rotation angle to each signal constellation to target the largest MIRD. Unfortunately, we find it considerably complicated to deduce closed-from results without brute-force search for the optimal rotation angles due to the differences in radii. Therefore, for practical use, we will still adopt the rotation angles solved with the same instantaneous subcarrier power constraint in Section III. As an example, for $\{\mathcal{S}_1, \ldots, \mathcal{S}_4\} = \{$QPSK-I, QPSK-II, BPSK-I, BPSK-II$\}$, the optimal four modes under the average subcarrier power constraint are shown in Fig. 3, whose associated radii, as calculated from Theorem 2, are $r_1 = 1.0321$, $r_1 = 1.0321$, $r_2 =$0.9326, and $r_2 = 0.9326$, respectively, and associated rotation angles, as calculated from Theorem 1, are $\theta_1 = 0$, $\theta_2 = \pi/6$, $\theta_3 = \pi/3$, and $\theta_4 = 5\pi/6$, respectively.

Table III lists the MIADs and MIRDs obtained from our proposed guidelines for four different sets of system parameters with the same instantaneous and average subcarrier power constraints, respectively, which are 1) SET 1: {QPSK-I, QPSK-II, BPSK-I, BPSK-II} ($\mathcal{F} = 2.5$ bps/Hz); 2) SET 2: {8-PSK, BPSK} ($\mathcal{F} = 2.5$ bps/Hz); 3) SET 3: {8-PSK-I, 8-PSK-II, QPSK-I, QPSK-II} ($\mathcal{F} = 3.5$ bps/Hz); 4) SET 4: {8-PSK-I, 8-PSK-II, 8-PSK-III, QPSK} ($\mathcal{F} = 3.75$ bps/Hz). Further, Fig. 4 compares the MIRDs for SETs 1-4 obtained from the extensive computer search and from our proposed guidelines. We observe from Fig. 4 that for the average subcarrier power constraint, our proposed guideline has a slight deviation from the optimal solution, while for the same instantaneous subcarrier power constraint it always provides the maximum MIRDs. Since the power allocation aims at the optimal asymptotic BER performance that mainly depends on the MIAD, employing power allocation always increases MIADs; however, it cannot necessarily guarantee larger MIRDs, which will be testified in Section VI.

V. Low-Complexity Receiver Design

The optimal ML detector of (6) requires the computation of 2^m metrics for each subcarrier group, which makes the implementation of GMM-OFDM-IM systems impractical. Motivated by the sequential decoding algorithm originally proposed for the convolutional codes [45]–[47], in this section, we propose a low-complexity detector for GMM-OFDM-IM systems, which exhibits near-optimal performance and avoids decisions on illegal mode permutations with much lower complexity. Since the detection for each subcarrier group is identical and independent, in what follows, we will only focus on the γ-th subcarrier group and omit the subscript (γ).

A. Sequential Detector

To begin with, we introduce an $n \times n$ matrix $\mathbf{B}$, whose (ς, τ)-th entry represents the most-likely transmitted symbol on the ς-th subcarrier when it employs $\mathcal{S}_\tau$

$$B_{\varsigma,\tau} = \arg\min_{s \in \mathcal{S}_\tau} |y(\varsigma) - s \cdot h(\varsigma)|^2, \quad \varsigma, \tau \in \mathcal{Q}, \tag{17}$$

and construct an $n \times n$ matrix $\mathbf{D}$ with

$$D_{\varsigma,\tau} = |y(\varsigma) - B_{\varsigma,\tau} h(\varsigma)|^2 \tag{18}$$

to store the optimal metrics. Then, the CTFs of n subcarriers are sorted according to their absolute values in decreasing order. Let us define $\Omega = \{\omega_1, \ldots, \omega_n\}$ for $|h(\omega_1)|^2 > \cdots > |h(\omega_n)|^2$, $\omega_\beta, \beta \in \mathcal{Q}$.

To apply the sequential detector, we build up the detecting tree in Fig. 5, which has $n-1$ stages following the order dictated in Ω. In this tree, each node at the $(\beta-1)$-th stage has $n+1-\beta$ successors that represent $n+1-\beta$ possible modes carried on the ω_β-th subcarrier along the path, where $\beta \in \{1, \ldots, n-1\}$, and each branch is labeled with the metric as well as the associated most-likely transmitted symbol. The aim of this sequential detector is to find a path from the tree that has the minimum cumulated metric and is legal. This search can be facilitated with a stack, of which each entry

TABLE III
COMPARISON OF MIADS AND MIRDS UNDER SAME INSTANTANEOUS AND AVERAGE SUBCARRIER POWER CONSTRAINTS

$\{\mathcal{S}_1, \ldots, \mathcal{S}_n\}$	Same instantaneous subcarrier power constraint		Average subcarrier power constraint		
	MIAD	MIRD	MIAD	MIRD	$\{r_1, \ldots, r_K\}$
SET 1: {QPSK-I, QPSK-II, BPSK-I, BPSK-II}	1.4142	0.5176	1.4596	0.5175	$\{1.0321, 0.9326\}$
SET 2: {8-PSK, BPSK}	0.7654	0.3902	0.7998	0.4348	$\{1.0450, 0.7949\}$
SET 3: {8-PSK-I, 8-PSK-II, QPSK-I, QPSK-II}	0.7654	0.2611	0.8055	0.2747	$\{1.0524, 0.8859\}$
SET 4: {8-PSK-I, 8-PSK-II, 8-PSK-III, QPSK}	0.7654	0.1960	0.7818	0.2002	$\{1.0215, 0.8599\}$

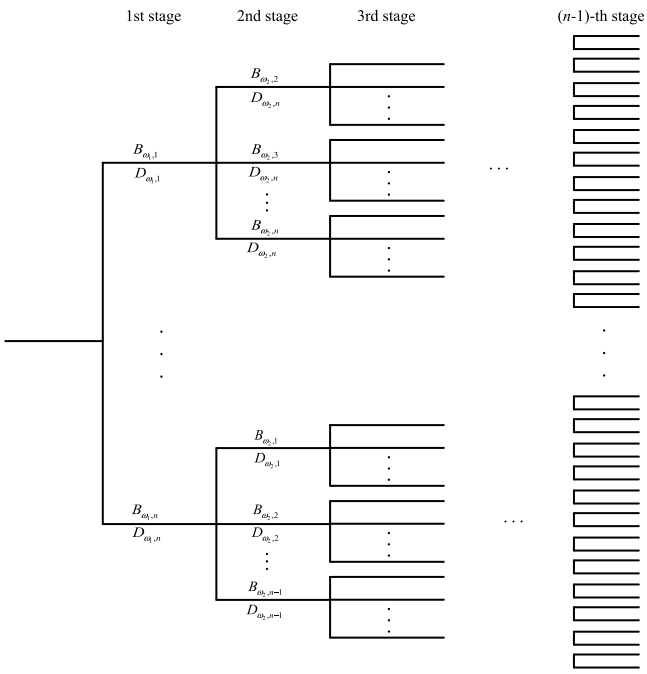

Fig. 5. Sequential detecting tree for GMM-OFDM-IM.

contains a path along with its cumulated metric and all entries are sorted in the order of increasing metric. Our idea is to always update the top path after adding its $n+1-\beta$ successors to the stack considering that it has the minimum ML metric until the top path reaches a length of n and passes the legality check.

The above-mentioned idea can be concretized by the proposed sequential detector, which is given by Algorithm 2. When the algorithm terminates, the top path in the stack is regarded as the estimated mode permutation. Meanwhile, the transmitted symbol on each subcarrier is obtained.

Example: Consider $(M_1(n_1), M_2(n_2)) = (4(2), 2(2))$ under the same instantaneous subcarrier power constraint, and suppose $\mathbf{B}$, $\mathbf{D}$, and Ω respectively are given by

$$\mathbf{B} = \begin{bmatrix} -1 & -e^{j\pi/6} & -e^{j\pi/3} & e^{j5\pi/6} \\ 1 & e^{j\pi/6} & e^{j\pi/3} & -e^{j5\pi/6} \\ j & e^{j4\pi/6} & e^{j\pi/3} & e^{j5\pi/6} \\ -1 & -e^{j\pi/6} & -e^{j\pi/3} & e^{j5\pi/6} \end{bmatrix}, \tag{19}$$

$$\mathbf{D} = \begin{bmatrix} 0.2392 & 0.1350 & 0.8475 & 0.4058 \\ 0.8181 & 0.8928 & 1.4398 & 0.1161 \\ 0.1017 & 0.0786 & 0.6312 & 0.2071 \\ 2.4050 & 2.5559 & 2.9861 & 2.5739 \end{bmatrix}, \tag{20}$$

Algorithm 2 Sequential Detector for GMM-OFDM-IM

1: Input: $\mathbf{y}$ and $\mathbf{h}$
2: Initialization: Calculate the matrices $\mathbf{B}$ and $\mathbf{D}$ by (17) and (18), respectively, and sort the CTFs of n subcarriers to obtain Ω;
3: Load the stack with the paths at the first stage of the tree and sort the stack in the order of increasing metric;
4: Replace the top path with its successors at the next stage of the tree, update the metric associated with the new paths, and rearrange the stack in the order of increasing metric;
5: **if** the length of the top path reaches n-1 **then**
6: Supplement the remaining one mode;
7: Examine the legality of the top path by a look-up table or (1);
8: **else**
9: Go to Step 4;
10: **end if**
11: **if** the top path is legal **then**
12: Stop;
13: **else**
14: Delete the top path;
15: Go to Step 4;
16: **end if**
17: Output: The top path in the stack

and $\Omega = \{2, 1, 3, 4\}$. From Algorithm 1, we have $\mathcal{S}_1 = \{1, j, -1, -j\}$, $\mathcal{S}_2 = \{e^{j\pi/6}, e^{j4\pi/6}, -e^{j\pi/6}, -e^{j4\pi/6}\}$, $\mathcal{S}_3 = \{e^{j\pi/3}, -e^{j\pi/3}\}$, and $\mathcal{S}_4 = \{e^{j5\pi/6}, -e^{j5\pi/6}\}$. The detecting process is shown in Fig. 6. After three loops, the detector outputs the final estimated mode permutation

$$\hat{\mathcal{I}} = \{4, 1, 2, 3\}, \tag{21}$$

and the associated symbols

$$\hat{\mathbf{s}} = \{-e^{j5\pi/6}, -1, e^{j4\pi/6}, -e^{j\pi/3}\}. \tag{22}$$

Note that as shown in Fig. 6(d), since the top path $(\{4, 2, 1\})$ in the stack at the end of loop 2 is not legal, it is deleted and the new top path $(\{4, 1\})$ is extended in Step 4.

B. Complexity Analysis and Difference from the Existing Detectors

The computational complexity of the sequential detector consists of two parts. The first part arises from the calculation of matrices $\mathbf{B}$ and $\mathbf{D}$, which is of order $\sim \mathcal{O}(n \sum_{k=1}^{K} n_k M_k)$. The second part is caused by the search of the optimal path in the tree, which mainly includes the computations involved

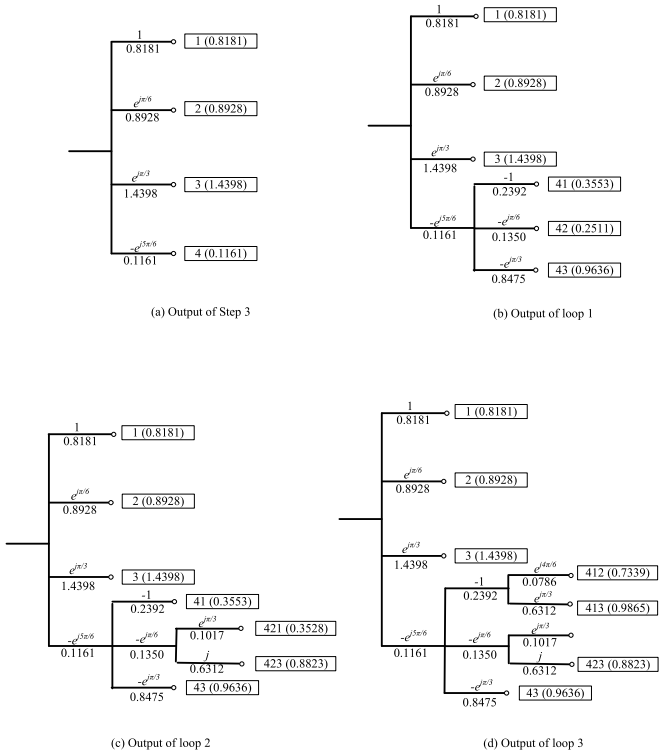

Fig. 6. An example of detecting process.

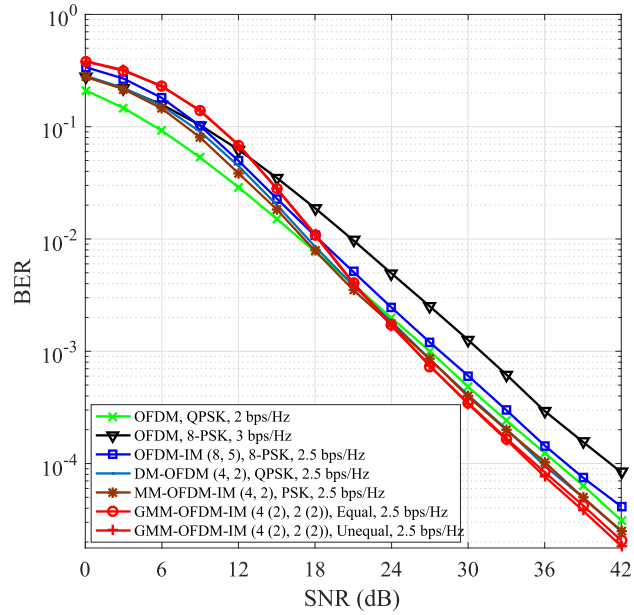

Fig. 7. Performance comparison among classical OFDM with QPSK/8-PSK, "OFDM-IM (8, 5), 8-PSK", "DM-OFDM (4, 2), QPSK", "MM-OFDM-IM (4, 2), PSK", and "GMM-OFDM-IM (4 (2), 2 (2)), Equal/Unequal".

in reordering the stack after every path extension. Since the sequential detector traces a somewhat random path back and forth through the tree, jumping from node to node, the total number of computations is a random variable. We should note that when the received signal is not too noisy, the trace process is likely to proceed forward continually without a backtrace and only $n-1$ rearrangements of the stack are required to obtain the optimal path.

Although our previously proposed MM-OFDM-IM(-IQ) detectors in [39], namely the low-complexity ML and subcarrier-wise detectors, are also applicable to GMM-OFDM-IM systems, the sequential detector has its unique features and advantages. For the low-complexity ML detector, the optimal mode permutation is derived by a Viterbi-like algorithm. All paths that merge at each node should be considered and at each node, one survival path with the minimum accumulated metric value should be kept for further consideration. By contrast, in the sequential detector, only the path with the minimum additive metric is extended and replaced by its successors. The sequential detector normally exhibits much fewer computations than the low-complexity ML detector except for the special case in which the received signal is heavily corrupted by noise. On the other hand, in comparison with the subcarrier-wise detector, the sequential detector is able to avoid illegal estimates for mode permutations. Therefore, the BER performance of the sequential detector is expected to be better than that of the subcarrier-wise detector, which will be validated in Section VI.

Remark: The sequential detector also applies to other OFDM-IM related schemes with inactive subcarriers by regarding "0" transmitted on the inactive subcarriers as a mode according to its general principle. Also note that the sequential detector becomes the ML detector if we always keep the stack sorted in the order of increasing metric and the top path of length n is legal.

VI. Simulation Results and Discussion

In this section, we perform Monte Carlo simulations to evaluate the uncoded BER performance of GMM-OFDM-IM systems and compare it with that of classical OFDM, OFDM-IM [9], and DM-OFDM systems [34]. All considered schemes operate over Rayleigh fading channels and perfect channel estimation is assumed at the receivers. For notational simplicity, the OFDM-IM scheme with a out of n subcarriers being active and transmitting M-PSK symbols is referred to as "OFDM-IM (n, a), M-PSK", the DM-OFDM scheme with a out of n subcarriers employing the primary M-ary PSK constellation as "DM-OFDM (n, a), M-PSK", the MM-OFDM-IM scheme with n subcarriers employing n different M-ary PSK constellations as "MM-OFDM-IM (M, n), PSK", and the GMM-OFDM-IM scheme with (without) instantaneous subcarrier power constraint and $n_1, \ldots, n_K$ subcarriers respectively employing $M_1, \ldots, M_K$-ary constellations as "GMM-OFDM-IM $(M_1(n_1), \ldots, M_K(n_K))$, Equal (Unequal)". It is worth noting that for fair comparisons, the DM-OFDM scheme also adopts our design guidelines to generate the optimal primary and secondary constellations.

A. Uncoded BER Performance

In this subsection, the uncoded BER performance comparisons are provided. All involved schemes employ the optimal ML detection.

Fig. 7 presents the comparison results among classical OFDM with QPSK/8-PSK, "OFDM-IM (8, 5), 8-PSK", "DM-OFDM (4, 2), QPSK", "MM-OFDM-IM (4, 2), PSK", and

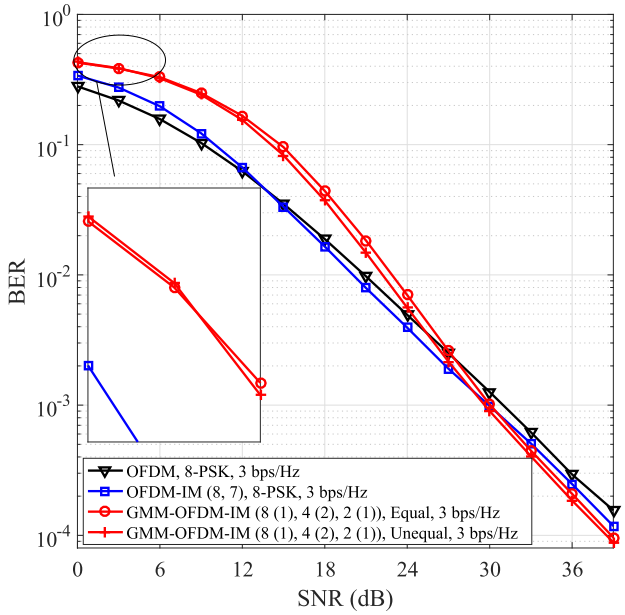

Fig. 8. Performance comparison among classical OFDM with 8-PSK, "OFDM-IM (8, 7), 8-PSK", and "GMM-OFDM-IM (8 (1), 4 (2), 2 (1)), Equal/Unequal".

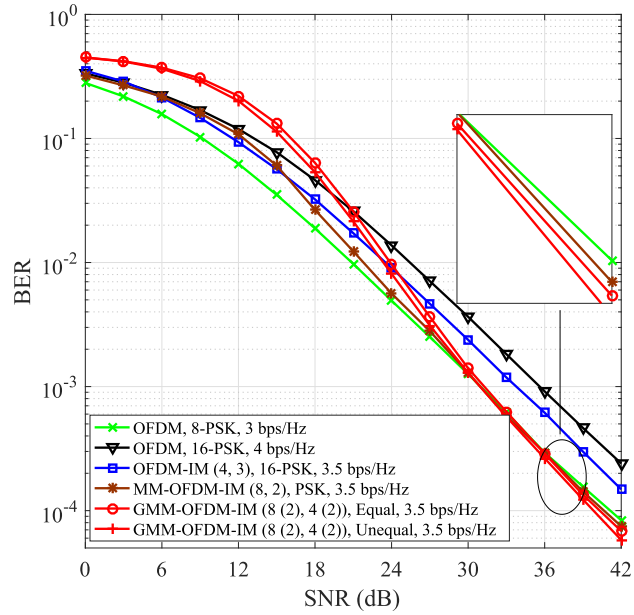

Fig. 9. Performance comparison among classical OFDM with 8/16-PSK, "OFDM-IM (4, 3), 16-PSK", "MM-OFDM-IM (8, 2), PSK", and "GMM-OFDM-IM (8 (2), 4 (2)), Equal/Unequal".

"GMM-OFDM-IM (4 (2), 2 (2)), Equal/Unequal", where all schemes achieve an SE of 2.5 bps/Hz except OFDM with QPSK (8-PSK) that has an SE of 2 (3) bps/Hz. Recall that the four modes employed by "GMM-OFDM-IM (4 (2), 2 (2))" are depicted in Fig. 3. As can be observed from Fig. 7, all schemes achieve the same diversity order of unity. While achieving a higher SE, OFDM-IM performs slightly worse than classical OFDM with QPSK; however, it acquires an SNR gain of about 3 dB over classical OFDM with 8-PSK. DM-OFDM, MM-OFDM-IM, and GMM-OFDM-IM outperform classical OFDM and OFDM-IM in the medium-to-high SNR region, verifying the advantages of using multiple signal constellations for IM. Specifically, MM-OFDM-IM performs slightly better than DM-OFDM at low SNR, while at high SNR, they almost achieve the same error performance due to the same proportion of IM bits. As stated in [26], the IM bits have a stronger protection than the ordinary modulation bits in the high SNR region, so that the IM bits are more likely to undergo error-free transmission at high SNR. The proportion of the IM bits in GMM-OFDM-IM is larger than that in other schemes, which alleviates the impact of the ordinary modulation bits on the BER more. Furthermore, following our design guidelines of mode selection, the ordinary modulation bits are mapped using the regular PSK constellations that achieve the optimal Euclidean distance. Therefore, GMM-OFDM-IM performs the best in the asymptotically high SNR region, and obtains approximately 1 dB SNR gain over DM-OFDM. On the other hand, it is obvious that employing power allocation improves the BER performance of GMM-OFDM-IM systems at high SNR. This is expected from Table III as the MIAD increases from 1.4142 to 1.4596. Due to very close resulting MIRDs, the BER curves of GMM-OFDM-IM with and without power allocation almost overlap in the low SNR region.

Fig. 8 compares the BER curves of classical OFDM with 8-PSK, "OFDM-IM (8, 7), 8-PSK", and "GMM-OFDM-IM (8 (1), 4 (2), 2 (1)), Equal/Unequal" at an SE of 3 bps/Hz. For the clarity of the figure, the BER curve of DM-OFDM has been removed. As shown in Fig. 8, OFDM-IM achieves an SNR gain of about 0.5 dB over classical OFDM. This is because a power saving factor of 12.5% is provided by OFDM-IM due to the presence of one inactive subcarrier out of eight available subcarriers and this corresponds to an SNR gain of $10\log_{10}8/7 \approx 0.58$ dB at high SNR. Although GMM-OFDM-IM performs worse than OFDM and OFDM-IM at low SNR because of a higher error probability of detecting mode permutations, it performs the best in the high SNR region among all schemes, achieving SNR gains of about 3 dB and 1.5 dB over classical OFDM and OFDM-IM, respectively. On the other hand, it is observed that "GMM-OFDM-IM (8 (1), 4 (2), 2 (1)), Unequal" is superior to "GMM-OFDM-IM (8 (1), 4 (2), 2 (1)), Equal" with the exception of very low SNR. This can be explained by the fact that GMM-OFDM-IM with power allocation leads to a larger MIAD yet a smaller MIRD than that without power allocation.

Fig. 9 shows the BER performance comparison among classical OFDM with 8/16-PSK, "OFDM-IM (4, 3), 16-PSK", "MM-OFDM-IM (8, 2), PSK", and "GMM-OFDM-IM (8 (2), 4 (2)), Equal/Unequal", where an SE of 3.5 bps/Hz is achieved by OFDM-IM, MM-OFDM-IM, and GMM-OFDM-IM, and 3 (4) bps/Hz by classical OFDM with 8-PSK (16-PSK). The BER curve of DM-OFDM is not included for the clarity of the figure. It can be seen from Fig. 9 that the BER curve of OFDM-IM lies between those of OFDM at 3 bps/Hz and 4 bps/Hz. Both GMM-OFDM-IM schemes outperform OFDM-IM and an SNR gain of about 3 dB is observed when SNR$\geq$ 33 dB. The asymptotic BER performance of GMM-OFDM-IM schemes perform better than MM-OFDM-IM, and

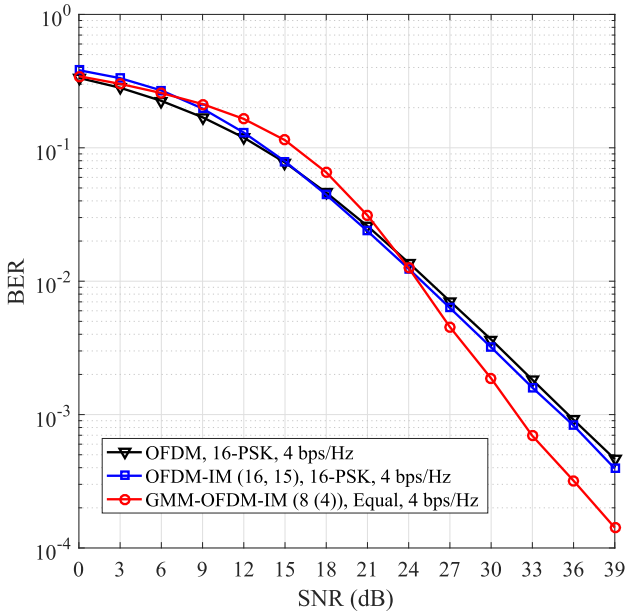

Fig. 10. Performance comparison among classical OFDM with 16-PSK, "OFDM-IM (16, 15), 16-PSK", and "GMM-OFDM-IM (8 (4)), Equal".

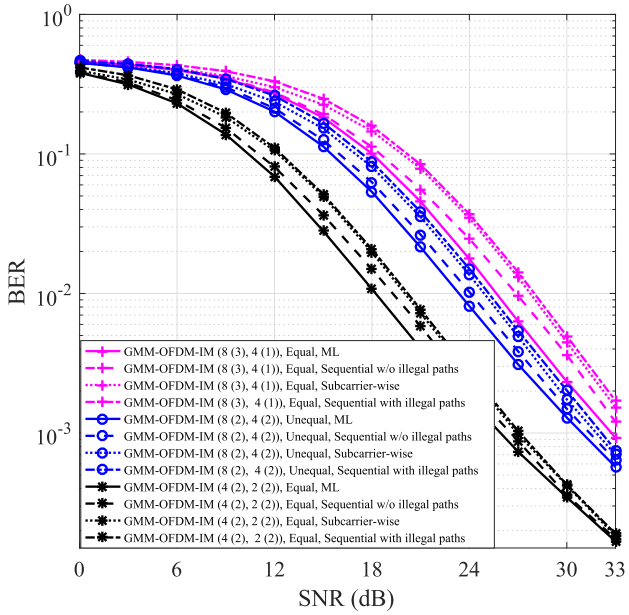

Fig. 11. Performance of the sequential detectors with/without illegal paths for "GMM-OFDM-IM (8 (3), 4 (1)), Equal", "GMM-OFDM-IM (8 (2), 4 (2)), Unequal", and "GMM-OFDM-IM (4 (2), 2 (2)), Equal".

is even superior to that of classical OFDM with 8-PSK, though they have a higher SE. This is because half of the total subcarriers in GMM-OFDM-IM are modulated by a lower-order signal constellation, and the loss of transmission rate in CM bits is compensated through a larger amount of IM bits that have a stronger protection. Moreover, since the power allocation enlarges not only the MIAD but also the MIRD as shown in Table III, GMM-OFDM-IM under the average subcarrier power constraint performs better than that under the same instantaneous subcarrier power constraint in the overall SNR region.

Fig. 10 depicts the BER performance of classical OFDM with 16-PSK, "OFDM-IM (16, 15), 16-PSK", and "GMM-OFDM-IM (8 (4)), Equal", where all schemes achieve an SE of 4 bps/Hz. It is observed from Fig. 10 that OFDM-IM achieves a marginal SNR gain over classical OFDM due to the small energy saving that arises from one inactive subcarrier in each subcarrier group. Since by embedding information onto the permutations of modes, a larger portion of bits can be transmitted via IM, and a lower-order signal constellation can be employed by each subcarrier in GMM-OFDM-IM. GMM-OFDM-IM performs the best among three schemes in the SNR region of interest, achieving an SNR gain of about 4 dB over classical OFDM and OFDM-IM.

B. Sub-Optimal Detection Performance

Fig. 11 illustrates the BER performance of the proposed sequential detectors with/without illegal paths, the subcarrier-wise detectors [39], and the optimal ML detectors for "GMM-OFDM-IM (8 (3), 4 (1)), Equal", "GMM-OFDM-IM (8 (2), 4 (2)), Unequal", and "GMM-OFDM-IM (4 (2), 2 (2)), Equal". It is observed from Fig. 11 that for all GMM-OFDM-IM systems, since decisions on illegal mode permutations are completely avoided, the sequential detectors without illegal paths perform better than the subcarrier-wise detectors for the entire SNR range. By contrast, the sequential detectors with illegal paths perform slightly worse than the subcarrier-wise detectors. On the other hand, the sequential detector suffers from a performance loss of approximately 1.5 dB in comparison with the ML detector in the medium SNR region. However, at both low and high SNR the sequential detector has the capability of achieving near-optimal performance. Recalling that the computational complexity of the sequential detector is intermediate between that of ML and subcarrier-wise detectors, the sequential detector provides a good trade-off between the error performance and the complexity.

VII. Conclusions and Remarks

In this paper, a novel OFDM transmission scheme, namely GMM-OFDM-IM, which allows a signal constellation of a different size to modulate different OFDM subcarriers, has been proposed. Aiming at the optimal asymptotic BER performance, design guidelines for GMM-OFDM-IM with or without the same instantaneous subcarrier power have been given. A low-complexity near optimal detector has been also tailored to GMM-OFDM-IM to facilitate the implementation. Monte Carlo simulation results have verified the effectiveness of the designs and demonstrated the advantages of GMM-OFDM-IM over the existing frequency-domain IM techniques. Note that the error performance of GMM-OFDM-IM can be further enhanced by extending to GMM-OFDM-IM-IQ which performs IM on the I- and Q- dimensions independently.

The following two points remain unsolved in this work: i) the efficient search for the optimal constellation rotation angles under the average subcarrier power constraint; ii) the optimal selection of the constellation sizes for different modes and

the number of subcarriers employing a specific mode under a given SE. Furthermore, GMM-OFDM-IM has the potential to be incorporated with cooperative networks that have been studied with OFDM-IM in [48] and [49].

REFERENCES

[1] E. Basar, "Index modulation techniques for 5G wireless networks," *IEEE Commun. Mag.*, vol. 54, no. 7, pp. 168–175, Jul. 2016.

[2] P. Yang, M. Di Renzo, Y. Xiao, S. Li, and L. Hanzo, "Design guidelines for spatial modulation," *IEEE Commun. Surveys Tuts.*, vol. 17, no. 1, pp. 6–26, 1st Quart., 2015.

[3] X. Cheng, M. Zhang, M. Wen, and L. Yang, "Index modulation for 5G: Striving to do more with less," *IEEE Wireless Commun. Mag.*, vol. 25, no. 2, pp. 126–132, Apr. 2018.

[4] E. Basar, M. Wen, R. Mesleh, M. Di Renzo, Y. Xiao, and H. Haas, "Index modulation techniques for next-generation wireless networks," *IEEE Access*, vol. 5, pp. 16693–16746, Sep. 2017.

[5] P. Yang *et al.*, "Single-carrier SM-MIMO: A promising design for broadband large-scale antenna systems," *IEEE Commun. Surveys Tuts.*, vol. 18, no. 3, pp. 1687–1716, 3rd Quart., 2016.

[6] M. Wen, X. Cheng, and L. Yang, *Index Modulation for 5G Wireless Communications*. Berlin, Germany: Springer, 2017.

[7] R. Abu-Alhiga and H. Haas, "Subcarrier-index modulation OFDM," in *Proc. IEEE 20th Int. Symp. Pers., Indoor Mobile Radio Commun. (PIMRC)*, Tokyo, Japan, Sep. 2009, pp. 177–181.

[8] D. Tsonev, S. Sinanovic, and H. Haas, "Enhanced subcarrier index modulation (SIM) OFDM," in *Proc. IEEE Global Commun. Conf. (GLOBECOM)*, Houston, TX, USA, Dec. 2011, pp. 728–732.

[9] E. Basar, U. Aygölü, E. Panayırcı, and H. V. Poor, "Orthogonal frequency division multiplexing with index modulation," *IEEE Trans. Signal Process.*, vol. 61, no. 22, pp. 5536–5549, Nov. 2013.

[10] M. Wen, Y. Zhang, J. Li, E. Basar, and F. Chen, "Equiprobable subcarrier activation method for OFDM with index modulation," *IEEE Commun. Lett.*, vol. 20, no. 12, pp. 2386–2389, Dec. 2016.

[11] Q. Ma, Y. Xiao, L. Dan, P. Yang, L. Peng, and S. Li, "Subcarrier allocation for OFDM with index modulation," *IEEE Commun. Lett.*, vol. 20, no. 7, pp. 1469–1472, Jul. 2016.

[12] J. Crawford, E. Chatziantoniou, and Y. Ko, "On the sep analysis of OFDM index modulation with hybrid low complexity greedy detection and diversity reception," *IEEE Trans. Veh. Technol.*, vol. 66, no. 9, pp. 8103–8118, Sep. 2017.

[13] A. I. Siddiq, "Low complexity OFDM-IM detector by encoding all possible subcarrier activation patterns," *IEEE Commun. Lett.*, vol. 20, no. 3, pp. 446–449, Mar. 2016.

[14] Y. Xiao, S. Wang, L. Dan, X. Lei, P. Yang, and W. Xiang, "OFDM with interleaved subcarrier-index modulation," *IEEE Commun. Lett.*, vol. 18, no. 8, pp. 1447–1450, Aug. 2014.

[15] X. Cheng, M. Wen, L. Yang, and Y. Li, "Index modulated OFDM with interleaved grouping for V2X communications," in *Proc. IEEE Int. Conf. Intell. Transp. Syst. (ITSC)*, Qingdao, China, Oct. 2014, pp. 1097–1104.

[16] M. Wen, X. Cheng, M. Ma, B. Jiao, and H. V. Poor, "On the achievable rate of OFDM with index modulation," *IEEE Trans. Signal Process.*, vol. 64, no. 8, pp. 1919–1932, Apr. 2016.

[17] N. Ishikawa, S. Sugiura, and L. Hanzo, "Subcarrier-index modulation aided OFDM—Will it work?" *IEEE Access*, vol. 4, pp. 2580–2593, Jun. 2016.

[18] Y. Ko, "A tight upper bound on bit error rate of joint OFDM and multi-carrier index keying," *IEEE Commun. Lett.*, vol. 18, no. 10, pp. 1763–1766, Oct. 2014.

[19] T. V. Luong and Y. Ko, "A tight bound on BER of MCIK-OFDM with greedy detection and imperfect CSI," *IEEE Commun. Lett.*, vol. 21, no. 12, pp. 2594–2597, Dec. 2017.

[20] T. Van Luong and Y. Ko, "Impact of CSI uncertainty on MCIK-OFDM: Tight closed-form symbol error probability analysis," *IEEE Trans. Veh. Technol.*, vol. 67, no. 2, pp. 1272–1279, Feb. 2018.

[21] Q. Ma, P. Yang, Y. Xiao, H. Bai, and S. Li, "Error probability analysis of OFDM-IM with carrier frequency offset," *IEEE Commun. Lett.*, vol. 20, no. 12, pp. 2434–2437, Dec. 2016.

[22] S. Gokceli, E. Basar, M. Wen, and G. K. Kurt, "Practical implementation of index modulation-based waveforms," *IEEE Access*, vol. 5, no. 1, pp. 25463–25473, Dec. 2017.

[23] M. Wen, X. Cheng, L. Yang, Y. Li, X. Cheng, and F. Ji, "Index modulated OFDM for underwater acoustic communications," *IEEE Commun. Mag.*, vol. 54, no. 5, pp. 132–137, May 2016.

[24] J. Zheng and R. Chen, "Linear processing for intercarrier interference in OFDM index modulation based on capacity maximization," *IEEE Signal Process. Lett.*, vol. 24, no. 5, pp. 683–687, May 2017.

[25] E. Basar, "OFDM with index modulation using coordinate interleaving," *IEEE Wireless Commun. Lett.*, vol. 4, no. 4, pp. 381–384, Aug. 2015.

[26] M. Wen, B. Ye, E. Basar, Q. Li, and F. Ji, "Enhanced orthogonal frequency division multiplexing with index modulation," *IEEE Trans. Wireless Commun.*, vol. 16, no. 7, pp. 4786–4801, Jul. 2017.

[27] J. Choi, "Coded OFDM-IM with transmit diversity," *IEEE Trans. Commun.*, vol. 65, no. 7, pp. 3164–3171, Jul. 2017.

[28] J. Choi and Y. Ko, "TCM for OFDM-IM," *IEEE Wireless Commun. Lett.*, vol. 7, no. 1, pp. 50–53, Feb. 2018.

[29] R. Fan, Y. J. Yu, and Y. L. Guan, "Generalization of orthogonal frequency division multiplexing with index modulation," *IEEE Trans. Wireless Commun.*, vol. 14, no. 10, pp. 5350–5359, Oct. 2015.

[30] B. Zheng, F. Chen, M. Wen, F. Ji, H. Yu, and Y. Liu, "Low-complexity ML detector and performance analysis for OFDM with in-phase/quadrature index modulation," *IEEE Commun. Lett.*, vol. 19, no. 11, pp. 1893–1896, Nov. 2015.

[31] E. Basar, "On multiple-input multiple-output OFDM with index modulation for next generation wireless networks," *IEEE Trans. Signal Process.*, vol. 64, no. 15, pp. 3868–3878, Aug. 2016.

[32] B. Zheng, M. Wen, E. Basar, and F. Chen, "Multiple-input multiple-output OFDM with index modulation: Low-complexity detector design," *IEEE Trans. Signal Process.*, vol. 65, no. 11, pp. 2758–2772, Jun. 2017.

[33] H. Zhang, L.-L. Yang, and L. Hanzo, "Compressed sensing improves the performance of subcarrier index-modulation-assisted OFDM," *IEEE Access*, vol. 4, pp. 7859–7873, Oct. 2016.

[34] T. Mao, Z. Wang, Q. Wang, S. Chen, and L. Hanzo, "Dual-mode index modulation aided OFDM," *IEEE Access*, vol. 5, pp. 50–60, Feb. 2017.

[35] T. Mao, Q. Wang, and Z. Wang, "Generalized dual-mode index modulation aided OFDM," *IEEE Commun. Lett.*, vol. 21, no. 4, pp. 761–764, Apr. 2017.

[36] X. Zhang, H. Bie, Q. Ye, C. Lei, and X. Tang, "Dual-mode index modulation aided OFDM with constellation power allocation and low-complexity detector design," *IEEE Access*, vol. 5, pp. 23871–23880, Nov. 2017.

[37] J. Zheng and R. Chen, "Achieving transmit diversity in OFDM-IM by utilizing multiple signal constellations," *IEEE Access*, vol. 5, pp. 8978–8988, Jun. 2017.

[38] T. Mao, Q. Wang, J. Quan, and Z. Wang, "Zero-padded orthogonal frequency division multiplexing with index modulation using multiple constellation alphabets," *IEEE Access*, vol. 5, pp. 21168–21178, Oct. 2017.

[39] M. Wen, E. Basar, Q. Li, B. Zheng, and M. Zhang, "Multiple-mode orthogonal frequency division multiplexing with index modulation," *IEEE Trans. Commun.*, vol. 65, no. 9, pp. 3892–3906, Sep. 2017.

[40] Q. Li, M. Wen, H. V. Poor, and F. Chen, "Information guided precoding for OFDM," *IEEE Access*, vol. 5, pp. 19644–19656, Oct. 2017.

[41] T. Keller and L. Hanzo, "Adaptive multicarrier modulation: A convenient framework for time-frequency processing in wireless communications," *Proc. IEEE*, vol. 88, no. 5, pp. 611–640, May 2000.

[42] S. Ye, R. Blum, and L. Cimini, "Adaptive OFDM systems with imperfect channel state information," *IEEE Trans. Wireless Commun.*, vol. 5, no. 11, pp. 3255–3265, Nov. 2006.

[43] Y. Rong, S. A. Vorobyov, and A. B. Gershman, "Adaptive OFDM techniques with one-bit-per-subcarrier channel-state feedback," *IEEE Trans. Commun.*, vol. 54, no. 11, pp. 1993–2003, Nov. 2006.

[44] M. K. Simon and M.-S. Alouini, *Digital Communication Over Fading Channels*, 2nd ed. New York, NY, USA: Wiley, 2005.

[45] J. M. Wozencraft, "Sequential decoding for reliable communication," *IRE Nat. Conv. Rec.*, vol. 5, no. 2, pp. 11–25, Aug. 1957.

[46] J. M. Wozencraft and B. Reiffen, *Sequential Decoding*. Cambridge, MA, USA: MIT Press, 1961.

[47] R. M. Fano, "A heuristic discussion of probabilistic decoding," *IEEE Trans. Inf. Theory*, vol. IT-9, no. 2, pp. 64–74, Apr. 1963.

[48] S. Dang, J. P. Coon, and G. Chen, "Adaptive OFDM with index modulation for two-hop relay-assisted networks," *IEEE Trans. Wireless Commun.*, vol. 17, no. 3, pp. 1923–1936, Mar. 2018.

[49] S. Dang, G. Chen, and J. P. Coon, "Power allocation for adaptive OFDM index modulation in cooperative networks," in *Proc. IEEE Globecom Workshops (GC Wkshps)*, Singapore, Dec. 2017, pp. 1–6.

Miaowen Wen (M'14–SM'18) received the B.S. degree from Beijing Jiaotong University, Beijing, China, in 2009, and the Ph.D. degree from Peking University, Beijing, China, in 2014. From 2012 to 2013, he was a Visiting Student Research Collaborator with Princeton University, Princeton, NJ, USA. He is currently an Associate Professor with the South China University of Technology, Guangzhou, China. He has published the book *Index Modulation for 5G Wireless Communications* (Springer) and over 90 research papers, which include over 50 journal papers and over 30 conference papers. His research interests include index modulation, non-orthogonal multiple access, physical layer security, and molecular communications.

Dr. Wen was a recipient of the Excellent Doctoral Dissertation Award from Peking University and the Best Paper Awards from the IEEE International Conference on Intelligent Transportation Systems Telecommunications in 2012, the IEEE International Conference on Intelligent Transportation Systems in 2014, and the IEEE International Conference on Computing, Networking and Communications (ICNC) in 2016. He was recognized as an Exemplary Reviewer for the IEEE COMMUNICATIONS LETTERS in 2017. He is currently serving as a Symposium Co-Chair for the IEEE ICNC 2019, a Workshop Co-Chair for the IEEE/CIC International Conference on Communications in China (ICCC 2018), and a Guest Editor for the IEEE JOURNAL ON SELECTED AREAS IN COMMUNICATIONS Special Issue on Spatial Modulation for Emerging Wireless Systems and the IEEE JOURNAL OF SELECTED TOPICS IN SIGNAL PROCESSING Special Issue on Index Modulation for Future Wireless Networks: A Signal Processing Perspective. He has served on the Editorial Boards of several international journals, including the IEEE ACCESS, the *EURASIP Journal on Wireless Communications and Networking*, the *ETRI Journal*, and the *Physical Communication* (Elsevier).

Ertugrul Basar (S'09–M'13–SM'16) received the B.S. degree (Hons.) from Istanbul University, Turkey, in 2007, and the M.S. and Ph.D. degrees from Istanbul Technical University, Turkey, in 2009 and 2013, respectively. From 2011 to 2012, he was with the Department of Electrical Engineering, Princeton University, Princeton, NJ, USA, as a Visiting Research Collaborator. He is currently an Associate Professor with the Department of Electrical and Electronics Engineering, Koç University, Istanbul, Turkey. Previously, he was an Assistant Professor and an Associate Professor with Istanbul Technical University from 2014 to 2017 and 2017 to 2018, respectively. He is an inventor of three pending/granted patents on index modulation schemes. His primary research interests include MIMO systems, index modulation, cooperative communications, OFDM, visible light communications, and signal processing for communications.

Recent recognition of his research includes the Science Academy (Turkey) Young Scientists (BAGEP) Award in 2018, the Turkish Academy of Sciences Outstanding Young Scientist (TUBA-GEBIP) Award in 2017, the first-ever IEEE Turkey Research Encouragement Award in 2017, and the Istanbul Technical University Best Ph.D. Thesis Award in 2014. He was also a recipient of five Best Paper Awards, including one from the IEEE International Conference on Communications 2016. He has served as a TPC track chair or a TPC member for several IEEE conferences, including GLOBECOM, VTC, PIMRC, and so on. He currently serves as an Editor for the IEEE TRANSACTIONS ON COMMUNICATIONS and *Physical Communication* (Elsevier), and an Associate Editor for the IEEE COMMUNICATIONS LETTERS. He served as an Associate Editor for the IEEE ACCESS from 2016 to 2018.

Qiang Li received the B.S. degree from the Inner Mongolia University of Science and Technology, Baotou, China, in 2013, and the M.S. degree from the Nanjing University of Aeronautics and Astronautics, Nanjing, China, in 2016. He is currently pursuing the Ph.D. degree with the South China University of Technology, Guangzhou, China. His recent research interests include MIMO systems, index modulation, and OFDM.

Wensong Zhang received the B.S. and M.S. degrees from the South China University of Technology, Guangzhou, China, in 2015 and 2018, respectively. His research interests include index modulation and OFDM.